

Article

Harmonic Spectrum of Output Voltage for Space Vector Pulse Width Modulated Ultra Sparse Matrix Converter

Tingna Shi * , Lingling Wu, Yan Yan and Changliang Xia 

School of Electrical and Information Engineering, Tianjin University, Tianjin 300072, China; wulingling@tju.edu.cn (L.W.); yanyan@tju.edu.cn (Y.Y.); motor@tju.edu.cn (C.X.)

* Correspondence: tnshi@tju.edu.cn; Tel.: +86-22-27402325

Received: 19 January 2018; Accepted: 2 February 2018; Published: 8 February 2018

Abstract: In a matrix converter, the frequencies of output voltage harmonics are related to the frequencies of input, output, and carrier signals, which are independent of each other. This nature may cause an inaccurate harmonic spectrum when using conventional analytical methods, such as fast Fourier transform (FFT) and the double Fourier analysis. Based on triple Fourier series, this paper proposes a method to pinpoint harmonic components of output voltages of an ultra sparse matrix converter (USMC) under space vector pulse width modulation (SVPWM) strategy. Amplitudes and frequencies of harmonic components are determined precisely for the first time, and the distribution pattern of harmonics can be observed directly from the analytical results. The conclusions drawn in this paper may contribute to the analysis of harmonic characteristics and serve as a reference for the harmonic suppression of USMC. Besides, the proposed method is also applicable to other types of matrix converters.

Keywords: ultra sparse matrix converter (USMC); space vector pulse width modulations (SVPWM); triple fourier series; harmonic analysis

1. Introduction

The ultra-sparse matrix converter (USMC) evolved from the conventional matrix converter (CMC) and inherited many merits from CMC including compact structure without intermediate storage, sinusoidal input and output current, adjustable input power factor, etc. Meanwhile, USMC possesses superiorities over CMC, such as simpler commutation technology, a decrease in number of switches, etc. Currently, USMC is considered as a promising type of matrix converter [1–4].

As an AC–AC power converter, the primary task of USMC is to obtain a sinusoidal output waveform with high quality. However, due to the characteristics of the power device and the modulation methods, the output voltages of USMC inevitably contain harmonic components, thus negatively impacting the practical application. Therefore, it is very important to analyze the harmonic components in the output waveform of USMC, which not only lays the foundation for the suppression of the harmonics but also improves the theory concerning matrix converter harmonic analysis.

Up to now, there are some studies on the harmonic analysis of power electronics converters. Among them, fast Fourier transform (FFT) analysis is the most commonly used one [5–8]. It is simple and easy to implement. However, FFT involves sampling and window etc. in the processing, which will incur spectrum leakage, aliasing, and other issues. Therefore, when the frequencies of input, output and carrier signals are special, the results of FFT analysis are not accurate. Another commonly used method is calculating the analytical formula with Fourier series. In 1975, S. Bayes and B.M. Bird first applied the double Fourier analysis method to power electronic converters which were originally used in the communication system [9]. Since then, the studies on harmonic analytic solution have

mostly concentrated on the double Fourier analysis. For example, the harmonic analytical formulas of output voltage of two-level inverter are derived in [10] by using double Fourier analysis and then a comparison about the high-frequency harmonics is carried out when using saw-tooth carrier and triangular carrier in modulation process. In [11], Jacobi matrix is used to find the closed solution of the double Fourier series; and the characteristics of output voltage of the inverter under different space vector pulse width modulation (SVPWM) are compared. In [12] the output voltage harmonics of inverters with different topologies under various modulation methods are analyzed in detail by double Fourier analysis.

Like CMC, the output voltage of USMC is related to the frequencies of input, output and carrier signals, which are independent of each other. If using double Fourier series analysis, only two of these frequencies are considered at most, resulting in inaccurate spectral analytic results. In view of this problem, some scholars have tried to use triple Fourier series to analyze the harmonic of output waveform for CMC under “AV method” [13,14]. However, due to some differences in the topology and control performance between USMC and CMC, a mature harmonic analysis theory for USMC has yet to emerge. Compared with “AV method”, SVPWM not only increases the maximum voltage transmission ratio from 0.5 to 0.866, but also achieves digitization easily. As a result, SVPWM is currently widely applied [15–17]. Therefore, for USMC, the harmonic analysis of output voltage under SVPWM is of important significance.

In this paper, based on the characteristics of SVPWM and triple Fourier series, an output voltage harmonic calculation method for USMC is proposed, which can obtain an accurate harmonic spectrum and identify the relations between the frequencies of harmonic components and the frequencies of input, output and carrier signals. In addition, the harmonic distribution pattern and the main harmonic components of output voltage of USMC are analyzed and summarized according to the analytical results.

2. Triple Fourier Series

It is assumed that the three-variable function $g(x, y, z)$ is periodic in x , y , and z directions with the period of 2π , x , y and z being independent of each other. The triple Fourier series expression of $g(x, y, z)$ can be defined by the following:

$$g(x, y, z) = \sum_{k=-\infty}^{+\infty} \sum_{p=-\infty}^{+\infty} \sum_{q=-\infty}^{+\infty} F_{kpq} e^{j(kx+py+qz)} \quad (1)$$

where k, p, q are indices on the carrier frequency, output frequency and input frequency respectively; F_{kpq} is the triple Fourier coefficient and its expression is

$$F_{kpq} = \frac{1}{8\pi^3} \int \int \int_0^{2\pi} g(x, y, z) e^{-j(kx+py+qz)} dx dy dz \quad (2)$$

Let $x = 2\pi f_c t$, $y = 2\pi f_{out} t + \phi_0$, $z = 2\pi f_{in} t + \phi_1$ then Equation (1) can be regarded as the output voltage expression of any phase of USMC; f_c, f_{out} and f_{in} are respectively carrier frequency, output voltage frequency and input voltage frequency of USMC; ϕ_1 is the input power factor angle; ϕ_0 is the output voltage initial phase. In most applications, USMC is required to operate with unit power factor, so $\phi_1 = 0$. When ϕ_0 is not zero, the integration limits of Equation (2) should be adjusted. Since the integrand $g(x, y, z)$ is periodic in x, y , and z directions with the period of 2π , the integration results would not be affected by the specific values of the integral limits as long as the periodic variation of x, y and z over 2π intervals. Therefore, whether ϕ_0 is zero does not have any effects on the calculation results. To simplify calculation, it is assumed that $\phi_0 = 0$.

Expanding Equation (1) and it can be expressed in the following form:

$$\begin{aligned}
 g(x, y, z) = \frac{A_{000}}{2} + & \left[\begin{aligned} & \sum_{k=1}^{+\infty} [A_{k00} \cos(kx) + B_{k00} \sin(kx)] + \\ & \sum_{p=1}^{+\infty} [A_{0p0} \cos(py) + B_{0p0} \sin(py)] + \\ & \sum_{q=1}^{+\infty} [A_{00q} \cos(qz) + B_{00q} \sin(qz)] \end{aligned} \right] \\
 + & \left[\begin{aligned} & \sum_{k=1}^{+\infty} \sum_{\substack{p=-\infty \\ p \neq 0}}^{+\infty} [A_{kp0} \cos(kx + py) + B_{kp0} \sin(kx + py)] + \\ & \sum_{p=1}^{+\infty} \sum_{\substack{q=-\infty \\ q \neq 0}}^{+\infty} [A_{0pq} \cos(py + qz) + B_{0pq} \sin(py + qz)] + \\ & \sum_{k=1}^{+\infty} \sum_{\substack{q=-\infty \\ q \neq 0}}^{+\infty} [A_{k0q} \cos(kx + qz) + B_{k0q} \sin(kx + qz)] \end{aligned} \right] \\
 + & \sum_{k=1}^{+\infty} \sum_{\substack{p=-\infty \\ p \neq 0}}^{+\infty} \sum_{\substack{q=-\infty \\ q \neq 0}}^{+\infty} \left[\begin{aligned} & A_{kpq} \cos(kx + py + qz) + \\ & B_{kpq} \sin(kx + py + qz) \end{aligned} \right]
 \end{aligned} \tag{3}$$

In Equation (3) harmonic components are divided into four parts: the first part is the DC component ($k = 0, p = 0, q = 0$); the second part is the fundamental voltage ($k = 0, p = 1, q = 0$) and harmonic components only associated with the carrier frequency (when $k = 1, 2, 3, \dots, p = 0, q = 0$), the input frequency (when $k = 0, p = 0, q = 1, 2, 3, \dots$) or the output frequency ($k = 0, p = 2, 3 \dots, q = 0$) respectively; the third part is the harmonic components related to any two of the three frequencies (input, output, and carrier frequencies), and their frequencies are the sum of the integral multiple of the two frequencies; the fourth part is the harmonic components relevant to the three frequencies, and their frequencies are sums of the integral multiples of the three frequencies.

According to the Fourier analysis theory, the frequency of any harmonic is $kf_c \pm pf_{\text{out}} \pm qf_{\text{in}}$ and the harmonic amplitude U_{kpq} satisfies the following relationship with F_{kpq} :

$$U_{kpq} = 2|F_{kpq}| \tag{4}$$

3. Harmonic Calculation of Output Voltage of USMC Under SVPWM Strategy

3.1. SVPWM

The topology of USMC is shown in Figure 1, which is divided into two stages, the rectifier stage and the inverter stage. There are three phases in rectifier stage, each of which consists of one unidirectional IGBT and four diodes. The inverter stage has the same structure as the traditional two-level voltage source inverter.

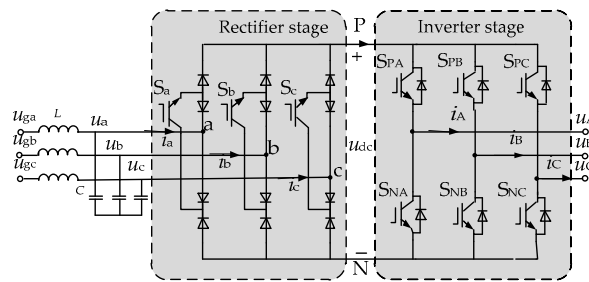


Figure 1. Typology of Ultra Sparse matrix converter.

The SVPWM strategy of rectifier stage is shown in Figure 2a, in which the six effective vectors I_1 – I_6 divide the space into six sectors. Taking $I_1(a, c)$ as an example, “a” represents that S_a and S_c are on-state, while S_b is off-state. In each sector, there is always one phase remaining the maximum current amplitude in the rectifier stage. In order to obtain the maximum voltage utilization, the switching device corresponding to maximum current amplitude is kept open, and the other two switches are switched on alternately. The duty cycles of the two adjacent effective vectors required to synthesize the reference input current vector I_{ref} can be obtained by the following equation:

$$\begin{cases} d_m = \frac{\sin[\frac{\pi}{3} - z - \frac{\pi}{6} + \frac{\pi}{3}(k_{in} - 1)]}{\cos[z - \frac{\pi}{3}(k_{in} - 1)]} \\ d_n = \frac{\sin[z + \frac{\pi}{6} - \frac{\pi}{3}(k_{in} - 1)]}{\cos[z - \frac{\pi}{3}(k_{in} - 1)]} \end{cases} \quad (5)$$

where k_{in} is the sector number of the reference input current vector.

When I_{ref} is in the first sector, the expression of average DC voltage u_{dc} in a carrier cycle is as follows:

$$u_{dc} = d_m u_{ab} + d_n u_{ac} = \frac{3U_{im}}{2 \cos z} \quad (6)$$

where u_{ab} and u_{ac} are input line voltage, $u_{ab} = \sqrt{3}U_{im} \cos(z + \pi/6)$, $u_{ac} = \sqrt{3}U_{im} \cos(z - \pi/6)$; U_{im} is the amplitude of input phase voltage.

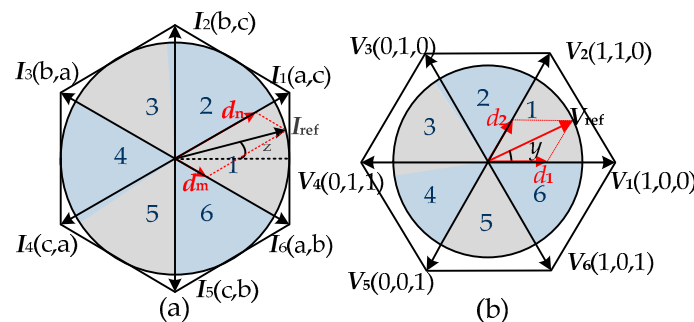


Figure 2. The space vector modulation strategy of Ultra Sparse matrix converter (a) rectifier stage (b) inverter stage.

Similarly, when I_{ref} is in other sectors, the values of u_{dc} and the duty cycles d_a , d_b and d_c of the switches S_a , S_b and S_c can be obtained as shown in Table 1.

Table 1. The expression of d_a , d_b , and d_c when I_{ref} in different vectors.

z	k_{in}	d_a	d_b	d_c	u_{dc}
$[-\pi/6, \pi/6)$	1	1	d_m	d_n	$3U_{im}/2\cos z$
$[\pi/6, \pi/2)$	2	d_m	d_n	1	$-3U_{im}/2\cos(z + 2\pi/3)$
$[\pi/2, 5\pi/6)$	3	d_n	1	d_m	$3U_{im}/2\cos(z - 2\pi/3)$
$[5\pi/6, 7\pi/6)$	4	1	d_m	d_n	$-3U_{im}/2\cos z$
$[7\pi/6, 3\pi/2)$	5	d_m	d_n	1	$3U_{im}/2\cos(z + 2\pi/3)$
$[3\pi/2, 11\pi/6)$	6	d_n	1	d_m	$-3U_{im}/2\cos(z - 2\pi/3)$

Figure 2b shows the SVPWM strategy of inverter stage, in which the six effective vectors V_1-V_6 divide the space vector into six sectors. Taking $V_1(1, 0, 0)$ as an example, “1” means that S_{PA} is on-state in the upper bridge arm of phase A; and the second and third bits “0” represent that S_{NB} and S_{NC} are turned on in the lower bridge arm of phase B and phase C respectively. The duty cycles of the two adjacent effective vectors and zero vectors required to synthesize the reference output voltage vector V_{ref} can be obtained by the following equation:

$$\begin{cases} d_1 = \frac{\sqrt{3}U_{ref}}{u_{dc}} \sin\left[\frac{\pi}{3} - y + \frac{\pi}{3}(k_{out} - 1)\right] \\ d_2 = \frac{\sqrt{3}U_{ref}}{u_{dc}} \sin\left[y - \frac{\pi}{3}(k_{out} - 1)\right] \\ d_0 = 1 - d_1 - d_2 \end{cases} \quad (7)$$

where k_{out} is the sector number of the reference output voltage vector, U_{ref} is the amplitude of output phase voltage.

The duty cycles of $S_{P\mu}$ ($\mu = A, B, C$) are defined as $d_{P\mu}$. When V_{ref} is located in different sectors, the values of $d_{P\mu}$ are shown in Table 2. Since the conducting state of upper and lower bridge arm switches in the same phase of A, B and C are complementary, the duty cycles of $S_{P\mu}$ and $S_{N\mu}$ satisfy the following relationship: $d_{N\mu} = 1 - d_{P\mu}$.

Table 2. The expression of $d_{P\mu}$ when V_{ref} is in different vectors.

y	k_{out}	d_{PA}	d_{PB}	d_{PC}
$[0, \pi/3)$	1	$(1 + d_1 + d_2)/2$	$(1 - d_1 + d_2)/2$	$(1 - d_1 - d_2)/2$
$[\pi/3, 2\pi/3)$	2	$(1 + d_1 - d_2)/2$	$(1 + d_1 + d_2)/2$	$(1 - d_1 - d_2)/2$
$[2\pi/3, \pi)$	3	$(1 - d_1 - d_2)/2$	$(1 + d_1 + d_2)/2$	$(1 - d_1 + d_2)/2$
$[\pi, 4\pi/3)$	4	$(1 - d_1 - d_2)/2$	$(1 + d_1 - d_2)/2$	$(1 + d_1 + d_2)/2$
$[4\pi/3, 5\pi/3)$	5	$(1 - d_1 + d_2)/2$	$(1 - d_1 - d_2)/2$	$(1 + d_1 + d_2)/2$
$[5\pi/3, 2\pi)$	6	$(1 + d_1 + d_2)/2$	$(1 - d_1 - d_2)/2$	$(1 + d_1 - d_2)/2$

3.2. Harmonic Calculation of Output Voltage

Since the three-phase output voltages of USMC are symmetrical, the following calculation and analysis take Phase A as an example. It can be seen from Equation (4) that the amplitude corresponding to each harmonic can be determined by the value of Fourier coefficients. Considering the SVPWM process, the integration limit can be redefined without altering the analytical solution, requiring only cyclic variation of x, y and z over 2π intervals. So the expression of F_{A_kpq} in Equation (2) can be defined as follows:

$$F_{A_kpq} = \frac{1}{8\pi^3} \int_{-\pi}^{\frac{11\pi}{6}} \int_0^{2\pi} \int_{-\pi}^{\pi} u_A e^{-j(kx+py+qz)} dx dy dz \quad (8)$$

In the operation process of USMC, u_A is actually a pulse wave. Therefore, to solve Equation (8), it is necessary to determine the trip point of the output voltage pulse and the value of u_A . The following is the process to solve various trip points of output voltage pulse based on the analysis of SVPWM of USMC.

When both the reference input current vector I_{ref} and output voltage vector V_{ref} are in the first sector, the conduction state of each switch in one carrier period and instantaneous value of A-phase output voltage can be determined based on the switching sequence of the rectification stage and the inverter stage, as shown in Figure 3.

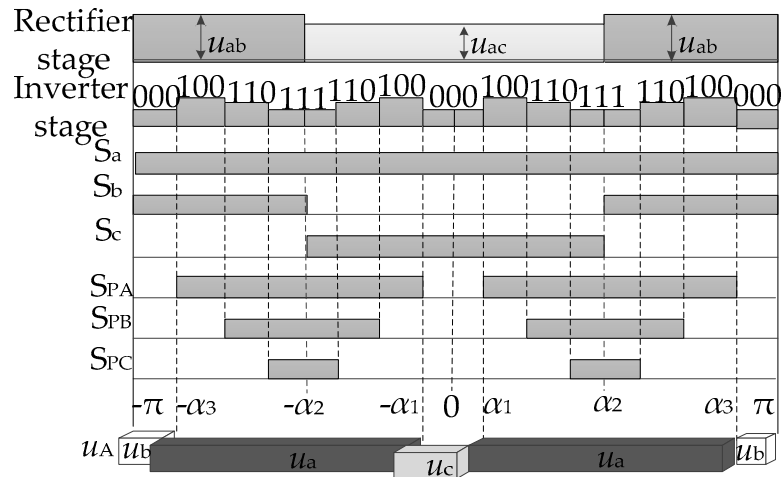


Figure 3. Modulation process when both I_{ref} and V_{ref} are in the first sector.

It should be noted that this paper is aimed at symmetrical regularly sampled SVPWM. The carrier function $c(x)$ used in this paper can be expressed as:

$$c(x) = \frac{1}{\pi} \cdot \arccos(\cos x), \quad x \in [-\pi, \pi] \tag{9}$$

Combine the duty cycle of each switch with Equation (9), and α_1, α_2 and α_3 in Figure 3 can be determined as follows:

$$\begin{cases} \alpha_1 = d_{NA}d_n = (1 - d_{PA})d_n\pi \\ \alpha_2 = d_n\pi \\ \alpha_3 = (d_n + d_{PA}d_m)\pi \end{cases} \tag{10}$$

When the reference vectors of input current and output voltage are located in other sectors, the values of α_1, α_2 and α_3 can be analyzed in a similar way. It is found that the expressions of α_1, α_2 and α_3 are the same when I_{ref} and V_{ref} are in different sectors, except that the specific values of d_{PA}, d_m and d_n are changed with k_{in} or k_{out} .

Based on the above analysis, Equation (8) can be further simplified as follows:

$$F_{A_kpq} = F_{A1} + F_{A2} \tag{11}$$

where

$$F_{A1} = \frac{1}{8\pi^3} \sum_{k_{in}=1,3,5} \sum_{k_{out}=1}^6 \int_{z_r}^{z_f} \int_{y_r}^{y_f} D_1 \cdot e^{-j(py+qz)} dydz \tag{12}$$

$$F_{A2} = \frac{1}{8\pi^3} \sum_{k_{in}=2,4,6} \sum_{k_{out}=1}^6 \int_{z_r}^{z_f} \int_{y_r}^{y_f} D_2 \cdot e^{-j(py+qz)} dydz \tag{13}$$

where

$$D_1 = \int_{-\pi}^{-\alpha_3} u_{A1} e^{-jkx} dx + \int_{-\alpha_3}^{-\alpha_1} u_{A2} e^{-jkx} dx + \int_{-\alpha_1}^{\alpha_1} u_{A3} e^{-jkx} dx + \int_{\alpha_1}^{\alpha_3} u_{A4} e^{-jkx} dx + \int_{\alpha_3}^{\pi} u_{A5} e^{-jkx} dx \tag{14}$$

$$\begin{aligned}
 D_2 = & \int_{-\pi}^{-\alpha_3} u_{A1} e^{-jkx} dx + \int_{-\alpha_3}^{-\alpha_2} u_{A2} e^{-jkx} dx + \int_{-\alpha_2}^{-\alpha_1} u_{A3} e^{-jkx} dx \\
 & + \int_{-\alpha_1}^{\alpha_1} u_{A4} e^{-jkx} dx + \int_{\alpha_1}^{\alpha_2} u_{A5} e^{-jkx} dx + \int_{\alpha_2}^{\alpha_3} u_{A6} e^{-jkx} dx \\
 & + \int_{\alpha_3}^{\pi} u_{A7} e^{-jkx} dx
 \end{aligned}
 \tag{15}$$

The integration limits z_r and z_f in Equations (12) and (13), and the values of $u_{A\lambda}$ ($\lambda = 1-7$) in Equations (14) and (15) are related to the sector number of reference input current as shown in Table 3.; y_r and y_f in Equations (12) and (13) are related to the sector number of reference output voltage, as shown in Table 4.

Table 3. Value of $u_{A\lambda}$, z_r and z_f when k_{in} changes from 1 to 6.

k_{in}	z_r	z_f	u_{A1}	u_{A2}	u_{A3}	u_{A4}	u_{A5}	u_{A6}	u_{A7}
1	$-\pi/6$	$\pi/6$	u_b	u_a	u_c	u_a	u_b	-	-
2	$\pi/6$	$\pi/2$	u_c	u_a	u_b	u_c	u_b	u_a	u_c
3	$\pi/2$	$5\pi/6$	u_c	u_b	u_a	u_b	u_c	-	-
4	$5\pi/6$	$7\pi/6$	u_a	u_b	u_c	u_a	u_c	u_b	u_a
5	$7\pi/6$	$3\pi/2$	u_a	u_c	u_b	u_c	u_a	-	-
6	$3\pi/2$	$11\pi/6$	u_b	u_c	u_a	u_b	u_a	u_c	u_b

Table 4. Value of y_r and y_f when k_{out} change from 1 to 6.

k_{out}	1	2	3	4	5	6
y_r	0	$\pi/3$	$2\pi/3$	π	$4\pi/3$	$5\pi/3$
y_f	$\pi/3$	$2\pi/3$	π	$4\pi/3$	$5\pi/3$	2π

Based on Equations (11) and (15), the analytical solution of F_{A_kpq} can be obtained by further calculation in MATLAB; then the amplitude of each harmonic can be got.

4. Spectrum Analysis of Harmonic Characteristics of Output Voltage of USMC

When the voltage transmission ratio m is 0.5 (m is the ratio of U_{ref}/U_{im}), the input frequency f_{in} is 50 Hz, the output frequency f_{out} is 70 Hz and the carrier frequency f_c is 5 kHz, the analytical spectrums of output phase voltage u_A and line voltage u_{AB} can be obtained by the calculation formula in Section 3. The spectrums are shown in Figure 4, where h_A and h_{AB} are normalized values based on the fundamental amplitude of phase voltage and line voltage respectively. It can be seen that the main harmonics are concentrated around the fundamental ($k = 0$) and 1 to 4 times of carrier frequency. Enlarge part of Figure 4 and mark the main harmonic frequency, as shown in Figure 5.

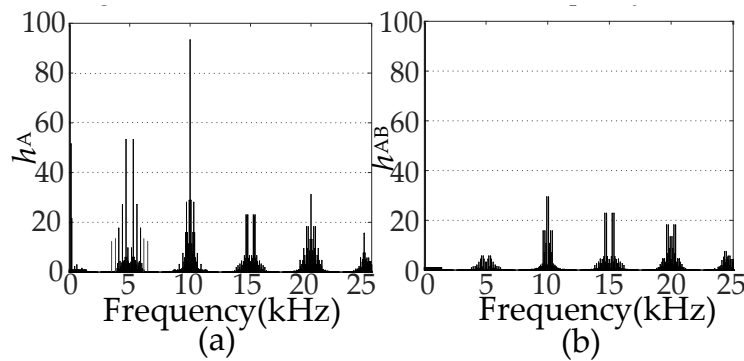


Figure 4. Theoretical spectral of output voltage ($m = 0.5$, $f_c = 5$ kHz, $f_{in} = 50$ Hz, $f_{out} = 70$ Hz) (a) spectrum of u_A (b) spectrum of u_{AB} .

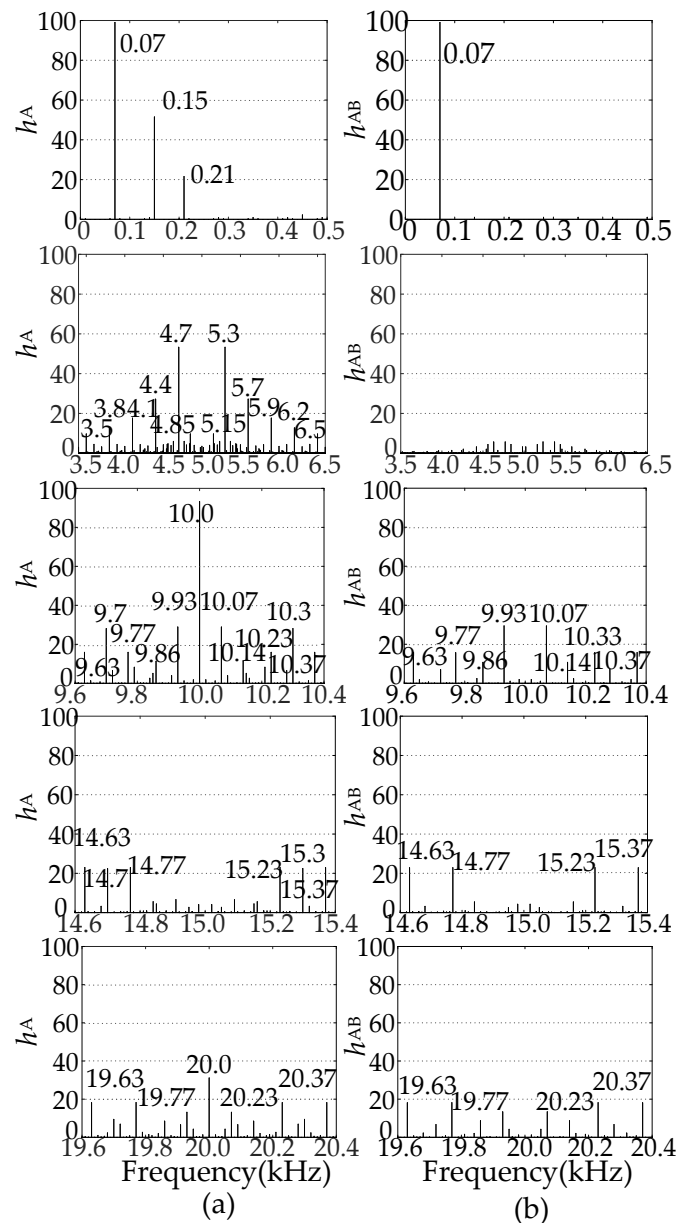


Figure 5. The partial enlargement of Figure 4 (a) spectral of u_A (b) spectral of u_{AB} .

From Figure 5, it can be seen that the main components of low-frequency harmonics in output phase voltage are $3f_{in}$ and $3f_{out}$. The amplitude of $3f_{in}$ is higher, which is up to 0.51 when $m = 0.5$. These two components belong to the common-mode voltage, so they are not contained in line voltage spectrum.

With respect to high-frequency harmonics, they cluster around an integer multiple of the carrier frequency and are symmetrical about the carrier frequency. Harmonics with high amplitudes in Figure 5 are listed in Table 5. The frequency expression of each harmonic in the table shows the relation between the frequency of main harmonics and the frequencies of input, output and carrier signals. Comparing the spectrum of phase voltage with line voltage, it is found that except the harmonics of $3f_{in}$ and $3f_{out}$, there are other harmonic components which also belong to the common mode voltage, as marked gray in Table 5. The amplitude of $2f_c$ is the highest among all the harmonic components, up to 0.93 under the condition of $m = 0.5$, followed by the component of $f_c \pm 6f_{in}$ with the amplitude of 0.53. According to literature [18–20], high-frequency common-mode voltages are the main cause of bearing damage, winding fault, electromagnetic interference. The above analysis can accurately

describe the amplitude of these common mode voltages, thus providing reference for the suppression of common mode voltage.

Table 5. The main harmonic components in high-frequency bands.

f (kHz)	f	h_A (%)
3.5/6.5	$f_c \pm 30f_{in}$	9.69
3.8/6.2	$f_c \pm 24f_{in}$	12.74
4.1/5.9	$f_c \pm 18f_{in}$	17.66
4.4/5.6	$f_c \pm 12f_{in}$	27.19
4.7/5.3	$f_c \pm 6f_{in}$	53.29
4.85/5.15	$f_c \pm 3f_{in}$	9.70
9.63/9.77/10.23/10.37	$2f_c \pm f_{out} \pm 6f_{in}$	15.91
9.7/10.3	$2f_c \pm 6f_{in}$	28.08
9.86/10.14	$2f_c \pm 2f_{out}$	11.31
9.93/10.17	$2f_c \pm f_{out}$	28.89
10.0	$2f_c$	93.32
14.63/14.77/15.23/15.37	$3f_c \pm f_{out} \pm 6f_{in}$	22.98
14.7/15.3	$3f_c \pm 6f_{in}$	22.50
19.63//19.77/20.23/20.37	$4f_c \pm f_{out} \pm 6f_{in}$	18.21
20.0	$4f_c$	31.13

According to Equations (11) to (15), the amplitude of each harmonic is related to the voltage transmission ratio m . When m increases from 0.1 to 0.8, the relationship between amplitudes of main harmonics and m can be obtained, as shown in Figure 6. The harmonics in Figure 6a are components except for the common mode voltage in the output phase voltage. It can be seen that except the harmonic of $2f_c \pm 2f_{out}$ most harmonics' amplitudes decrease when m increase. The harmonics in Figure 6b are common mode components. When $m \leq 0.5$, the amplitudes of $2f_c$, $f_c \pm 6f_{in}$, $3f_{in}$ and $3f_c \pm 6f_{in}$, are much higher than those of other harmonics. Besides, their amplitudes decrease rapidly with the increase of m . When $m > 0.5$, the amplitudes of harmonics in Figure 6b are gradually approaching, but still decrease with the increase of m .

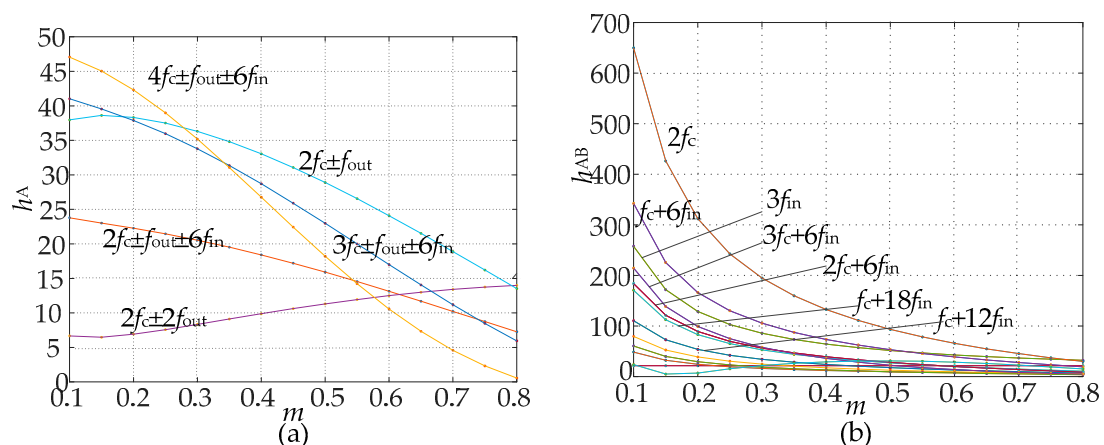


Figure 6. The relationship between main harmonic components and m in output phase voltage (a) components other than common mode voltage (b) common mode components.

From the above analysis, it can be seen that the amplitudes of high-frequency common mode components are much higher than those of other harmonics, especially when m is low. Besides, the harmonics' amplitudes are affected by the value of m . Most harmonics' amplitudes decrease gradually with the increase of m , but a few increase.

5. Comparative Analysis with FFT

The spectrums of the experimental waveforms cannot be obtained based on the triple Fourier series by the existing measurement techniques and analysis tools. FFT is usually used to deal with the experimental waveforms. Since it is very sensitive to the periodicity and frequency resolution of the waveforms, when the frequencies of input, output and carrier signals are all integers, and the time interval over which FFT is conducted as an integer multiple of the period of these three signals, the results obtained by the FFT analysis are accurate. However, when the values of these three frequencies are special (for example, the multiplicities of the three frequencies' reciprocals are large or the three frequencies include non-integer), it is difficult to ensure that the time is an integer multiple of the carrier cycle, input and output voltage cycle. Under this condition, the harmonic spectrums obtained by FFT are not accurate. The following are the examples.

The spectrums obtained by FFT on the experimental waveforms of output voltage are compared with those analytical results based on the method proposed in this paper. Figure 7 shows the USMC experimental system. When the amplitude of input phase voltage is 42 V and the voltage transmission ratio m is 0.5, $f_{in} = 50$ Hz, $f_{out} = 70$ Hz, $f_c = 5$ kHz. The time domain waveforms of output voltage and their FFT results are shown in Figure 8, where Figure 8a denotes the waveform of phase voltage u_A and its FFT results and Figure 8b denotes the waveform of line voltage u_{AB} and its FFT results. The amplitudes of all the harmonic components in Figure 8 are the nominal value based on the fundamental amplitude. The FFT results in Figure 8 cuts out a section of the output voltage waveform for seven output voltage periods with a frequency resolution of 10 Hz. From the magnitudes of f_{in} , f_{out} , and f_c , the time corresponding to seven output voltage periods is an integer multiple of the carrier, input and output period so the FFT results are accurate. The main harmonic components in Figure 8 are listed in Table 6 and compared with the results obtained from the analytical calculation. It can be seen that the frequencies of primary harmonics in Figure 8 are consistent with the analytical results but the amplitudes of them are slightly different. This is due to the existence of the switching dead-time, the conduction voltage drop of the switching device and the ripple of the input voltage at line side. The largest error between the measured spectrum and the theoretical results is only 3.06%.

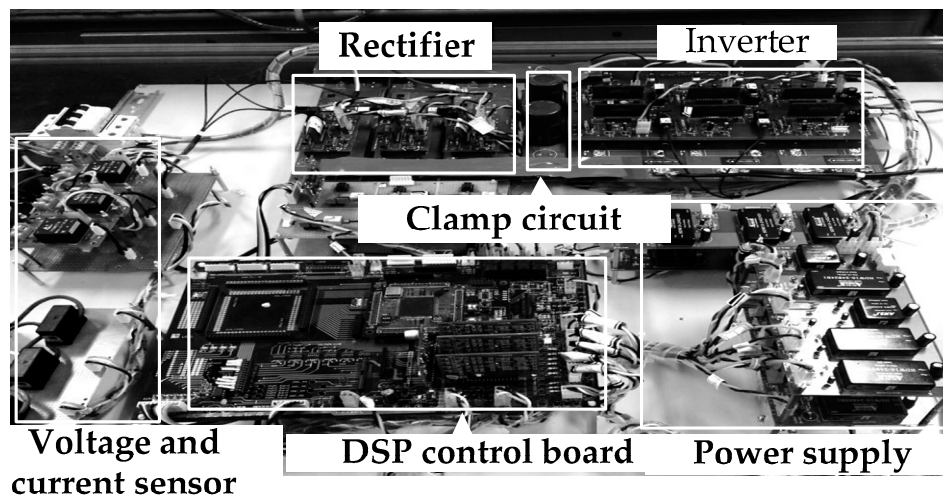


Figure 7. Experimental system of ultra-sparse matrix converter (USMC).

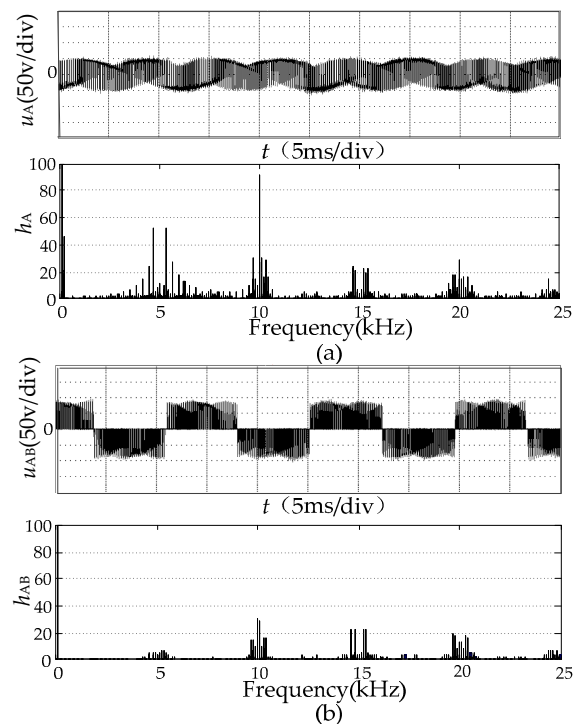


Figure 8. Time domain waveforms of output voltage and their FFT results (a) u_A and its FFT (b) u_{AB} and its FFT.

Table 6. The main harmonic components in Figure 8.

FFT Results		Analytical Results	
f (kHz)	h_A (%)	f (kHz)	h_A (%)
0.15	49.54	0.15	51.51
0.21	20.73	0.21	21.51
3.5/6.5	9.56	3.5/6.5	9.69
3.8/6.2	11.69	3.8/6.2	12.74
4.1/5.9	18.18	4.1/5.9	17.66
4.4/5.6	25.72	4.4/5.6	27.19
4.7/5.3	51.07	4.7/5.3	53.29
4.85/5.15	10.17	4.85/5.15	9.70
9.63/9.77/10.23/10.77	14.50	9.63/9.77/10.23/10.77	15.90
9.7/10.3	30.40	9.7/10.3	28.06
9.86/10.14	12.14	9.86/10.14	11.31
9.93/10.07	27.45	9.93/10.07	28.89
10.0	90.26	10.0	93.32
14.63/14.77/15.23/15.37	23.07	14.63/14.77/15.23/15.37	22.98
14.7/15.3	24.36	14.7/15.3	22.50
19.63/19.77/20.23/20.37	19.07	19.63/19.77/20.23/20.37	18.21
20.00	28.20	20.00	31.13

When $f_{in} = 50$ Hz, $f_{out} = 70.5$ Hz, $f_c = 5$ kHz, $m = 0.5$, the output voltage harmonic spectrums are shown in Figure 9. Under this condition, at least 141 periods of output waveform has to be intercepted to ensure the accuracy of FFT results. But the amount of data corresponding to 141 output periods is too large to be processed. The FFT results in Figure 9 intercepted a section of the output voltage waveform for seven output voltage periods with the frequency resolution of 10.07 Hz, it can be seen that there exist large errors between the FFT analysis and the analytical results. However, the analytic calculation method based on triple Fourier series in this paper is not affected by the magnitude of

input, output and carrier frequencies. The analytical results can accurately determine the amplitudes and frequency of each harmonic component regardless of the magnitude of the three frequencies. In practical applications, the carrier frequency and the output frequency of USMC usually vary according to application requirements. Therefore, the method proposed in this paper has a wider scope of application than FFT.

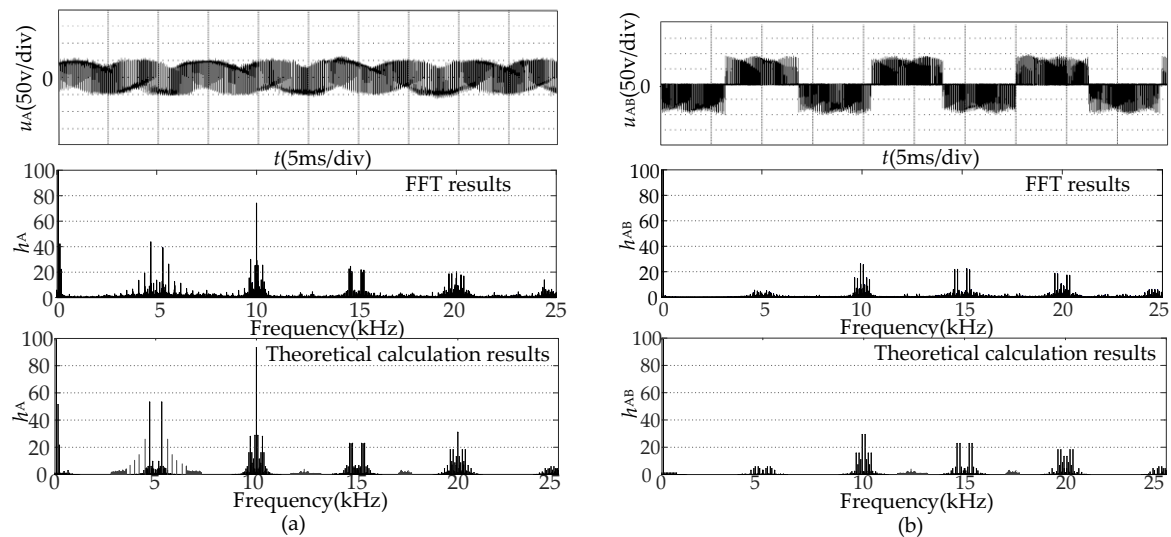


Figure 9. Time domain waveforms of output voltage and their spectrum ($m = 0.5$, $f_{in} = 50$ Hz, $f_{out} = 70.5$ Hz, $f_c = 5$ kHz) (a) u_A and its spectrum (b) u_{AB} and its spectrum.

6. Conclusions

In this paper, a theoretical calculation method based on three Fourier series is proposed for USMC under SVPWM. Taking input, output, and carrier frequencies into account, amplitudes and frequencies of harmonic components of output voltage are determined precisely for the first time. Including both the low-frequency harmonics and the high-frequency harmonic components, the relation between the frequencies of harmonic components and the frequencies of input, output and carrier signals can be determined. Through spectrum analysis in this paper, the following conclusions can be drawn:

1. The frequencies of low-frequency harmonics are triple that of the input or output frequencies. The high-frequency harmonics are organized in sidebands and symmetrical about integer multiples of carrier frequency.
2. The high-frequency common-mode components are $kf_c + 6f_{in}$, kf_c , etc., whose amplitudes are high. This feature is obvious, especially when the voltage transmission m is low.
3. The harmonic amplitudes are affected by the value of m , and most of which decrease gradually with the increase of m , while a few decrease.

Acknowledgments: The authors are grateful to the financial support from the National Natural Science Foundation of China under Grant 51777135 and the Application Foundation and Front Technology Research Program of Tianjin under Grant 15JCQNJC04300.

Author Contributions: Tingna Shi, Lingling Wu, and Changliang Xia put forward the idea; Lingling Wu and Yan Yan performed the experiments and analyzed the results; all authors contributed to the writing of the paper.

Conflicts of Interest: The authors declare no conflict of interest.

References

1. Kolar, J.W.; Schafmeister, F.; Round, S.D.; Ertl, H. Novel three-phase AC–AC sparse matrix converters. *IEEE Trans. Power Electron.* **2007**, *22*, 1649–1661. [[CrossRef](#)]

2. Siami, M.; Khaburi, D.A.; Rivera, M.; Rodriguez, J. An Experimental Evaluation of Predictive Current Control and Predictive Torque Control for a PMSM fed by a Matrix Converter. *IEEE Trans. Ind. Electron.* **2017**, *64*, 8459–8471. [[CrossRef](#)]
3. Shi, T.N.; Zhang, X.; An, S.B.; Yan, Y.; Xia, C.L. Harmonic suppression modulation strategy for ultra-sparse matrix converter. *IET Power Electron.* **2016**, *9*, 589–599. [[CrossRef](#)]
4. Tuyen, N.D.; Dzung, P.Q. Space Vector Modulation for an Indirect Matrix Converter with Improved Input Power Factor. *Energies* **2017**, *10*, 588. [[CrossRef](#)]
5. Qi, C.; Chen, X.; Qiu, Y. Carrier-based randomized pulse position modulation of an indirect matrix converter for attenuating the harmonic peaks. *IEEE Trans. Power Electron.* **2013**, *28*, 3539–3548. [[CrossRef](#)]
6. Sun, P.; Wang, X.; Hu, Y.; Xie, C.; Ning, L. The harmonic analysis and the arm capacitor parameters selection of module multilevel matrix converter. In Proceedings of the IEEE PES Asia-Pacific Power and Energy Engineering Conference (APPEEC), Xi'an, China, 25–28 October 2016; pp. 1617–1621. [[CrossRef](#)]
7. Wang, H.; Su, M.; Sun, Y.; Zhang, G.; Yang, J.; Gui, W.; Feng, J. Topology and Modulation Scheme of a Three-Level Third-Harmonic Injection Indirect Matrix Converter. *IEEE Trans. Ind. Electron.* **2017**, *64*, 7612–7622. [[CrossRef](#)]
8. Kim, S.; Yoon, Y.D.; Sul, S.K. Pulsewidth modulation method of matrix converter for reducing output current ripple. *IEEE Trans. Power Electron.* **2010**, *25*, 2620–2629. [[CrossRef](#)]
9. Bowes, S.R.; Bird, B.M. Novel approach to the analysis and synthesis of modulation processes in power convertors. *IET Proc. Inst. Electr. Eng.* **1975**, *122*, 507–513. [[CrossRef](#)]
10. Hamman, J.; Van Der Merwe, F.S. Voltage harmonics generated by voltage-fed inverters using PWM natural sampling. *IEEE Trans. Power Electron.* **1988**, *3*, 297–302. [[CrossRef](#)]
11. Moynihan, J.F.; Egan, M.G.; Murphy, J.M.D. Theoretical spectra of space-vector-modulated waveforms. *IEE Proc.-Electr. Power Appl.* **1998**, *145*, 17–24. [[CrossRef](#)]
12. Holmes, D.G.; Lipo, T.A. *Pulse Width Modulation for Power Converters: Principles and Practice*; John Wiley & Sons: Hoboken, NJ, USA, 2003.
13. Wang, B.; Sherif, E. Spectral analysis of matrix converters based on 3-D fourier integral. *IEEE Trans. Power Electron.* **2013**, *28*, 19–25. [[CrossRef](#)]
14. Wang, B.; Sherif, E. Analytical characterization of the spectral performance of matrix converters. In Proceedings of the Power Electronics and Motion Control Conference (IPEMC), Harbin, China, 2–5 June 2012; pp. 678–682. [[CrossRef](#)]
15. Rodriguez, J.; Rivera, M.; Kolar, J.W.; Wheeler, P.W. A review of control and modulation methods for matrix converters. *IEEE Trans. Ind. Electron.* **2012**, *59*, 58–70. [[CrossRef](#)]
16. Wang, X.; Lin, H.; She, H.; Feng, B. A research on space vector modulation strategy for matrix converter under abnormal input-voltage conditions. *IEEE Trans. Ind. Electron.* **2012**, *59*, 93–104. [[CrossRef](#)]
17. You, K.; Xiao, D.; Rahman, M.F.; Uddin, M.N. Applying reduced general direct space vector modulation approach of AC–AC matrix converter theory to achieve direct power factor controlled three-phase AC–DC matrix rectifier. *IEEE Trans. Ind. Appl.* **2014**, *50*, 2243–2257. [[CrossRef](#)]
18. Qu, J.; Xu, L.; Wang, L.; Qiu, L.; Li, Y. The modulation of common mode voltage suppression for a three-level matrix converter. In Proceedings of the IEEE International Conference on Aircraft Utility Systems, Beijing, China, 10–12 October 2016; pp. 533–538. [[CrossRef](#)]
19. Shi, T.N.; Huang, Q.Y.; Yan, Y.; Xia, C.L. Suppression of common mode voltage for matrix converter based on improved double line voltage synthesis strategy. *IET Power Electron.* **2014**, *7*, 1384–1395. [[CrossRef](#)]
20. Tran, Q.H.; Lee, H.H. A Three-Vector Modulation Strategy for Indirect Matrix Converter Fed Open-End Load to Reduce Common-Mode Voltage with Improved Output Performance. *IEEE Trans. Power Electron.* **2017**, *32*, 7904–7915. [[CrossRef](#)]

